sensors

MDPI

Communication

High Selectivity Hydrogen Gas Sensor Based on WO_3/Pd-AlGaN/GaN HEMTs

Van Cuong Nguyen, Ho-Young Cha and Hyungtak Kim *

School of Electronic and Electrical Engineering, Hongik University, Seoul 04066, Republic of Korea
* Correspondence: hkim@hongik.ac.kr; Tel.: +82-2-320-3013

Abstract: We investigated the hydrogen gas sensors based on AlGaN/GaN high electron mobility transistors (HEMTs) for high temperature sensing operation. The gate area of the sensor was functionalized using a 10 nm Pd catalyst layer for hydrogen gas sensing. A thin WO_3 layer was deposited on top of the Pd layer to enhance the sensor selectivity toward hydrogen gas. At 200 °C, the sensor exhibited high sensitivity of 658% toward 4%-H_2, while exhibiting only a little interaction with NO_2, CH_4, CO_2, NH_3, and H_2S. From 150 °C to 250 °C, the 10 ppm hydrogen response of the sensor was at least eight times larger than other target gases. These results showed that this sensor is suitable for H_2 detection in a complex gas environment at a high temperature.

Keywords: hydrogen sensor; gallium nitride; selectivity; palladium catalyst; tungsten trioxide; high electron mobility transistor

Citation: Nguyen, V.C.; Cha, H.-Y.; Kim, H. High Selectivity Hydrogen Gas Sensor Based on WO_3/Pd-AlGaN/GaN HEMTs. *Sensors* **2023**, *23*, 3465. https://doi.org/10.3390/s23073465

Academic Editors: Francesca Rolle, Pier Giorgio Spazzini and Aline Piccato

Received: 14 February 2023
Revised: 19 March 2023
Accepted: 24 March 2023
Published: 26 March 2023

1. Introduction

It is predicted that the Earth is facing a critical global warming situation. If the average temperature rises by 1.5 °C above pre-industrial levels, it will result in severe and permanent consequences such as climate change, loss of plant and animal species, food shortages, and environmental contamination [1–6]. The main cause of global warming is the increase in greenhouse gas emissions when people do not stop exploiting and consuming fossil fuels, such as petroleum, natural gas, and coal, which cause the concentration of CO_2 in the air to increase rapidly. As a result, the CO_2 levels increased from 316 ppm in 1960 to 417 ppm in 2020, as measured at Mauna Loa Observatory, Hawaii [7]. The global average surface temperature increased by about 0.6 °C over the 20th century [8,9]. The consequences of global warming are not something in the distant future, but are already clearly evident. In response to global warming, the use of environmentally friendly, zero-emission fuels that do not release greenhouse gases is more urgent than ever. Renewable energy sources such as solar, wind, and hydropower are being increasingly utilized to reduce greenhouse gas emissions. However, the intermittent nature of these sources and the lack of effective energy storage systems limit their widespread adoption. Hydrogen, on the other hand, emerged as a promising zero-emission fuel that can be produced from renewable sources and has a high energy density, making it an ideal candidate for energy storage and transportation.

Hydrogen can be produced through several methods, including electrolysis, biomass gasification, and steam methane reforming. Electrolysis, which involves splitting water into hydrogen and oxygen using electricity, is considered the most environmentally friendly method of hydrogen production when powered by renewable energy sources such as wind and solar. The use of renewable energy sources to produce hydrogen can help reduce greenhouse gas emissions and contribute to the transition to a low-carbon economy.

Hydrogen can be used in various applications, including transportation, heating, and power generation. In the transportation sector, hydrogen fuel cell electric vehicles (FCEVs) gained popularity due to their high efficiency, long range, and zero emissions. FCEVs use

hydrogen as a fuel to generate electricity, producing only water as a byproduct. In the heating sector, hydrogen can be used in fuel cells to provide combined heat and power for buildings, reducing greenhouse gas emissions from heating. Moreover, hydrogen can be used in industrial processes such as steel and chemical production, where hydrogen can replace fossil fuels as a feedstock, reducing greenhouse gas emissions from these sectors.

Despite the benefits of hydrogen as a zero-emission fuel, its production, storage, and transportation still face challenges. The development of low-cost and efficient hydrogen production methods, safe and efficient hydrogen storage systems, and reliable hydrogen transportation systems are critical to the widespread adoption of hydrogen as a mainstream energy source.

Hydrogen garnered significant attention in recent years as an alternative to fossil fuels, due to its eco-friendliness and abundance. However, the practical application of hydrogen fuel presents a significant challenge. The molecule's small size (0.289 nm), colorless and odorless nature, and high diffusion coefficient (0.61 cm^2/s) make it difficult to detect, store, and transport safely. Additionally, its broad flammability range (4–75%) poses a significant safety risk.

Despite these challenges, hydrogen fuel is widely used in various industries, including factories, rockets, automobiles, and metallurgy. However, storing hydrogen gas in high-pressure tanks can lead to significant safety risks due to the potential for explosions caused by even the tiniest leakage.

Therefore, developing a reliable and robust hydrogen gas sensor is crucial to ensure safe storage and transportation of hydrogen fuel. A high-quality sensor must possess high sensitivity and accuracy, a fast response time, and the ability to withstand harsh environments.

To address these challenges, researchers are developing novel hydrogen gas sensors using advanced materials and technology. For instance, metal oxide semiconductors were used as sensing materials due to their high sensitivity to hydrogen gas. Additionally, nanomaterials such as carbon nanotubes, graphene, and metal-organic frameworks were investigated as sensing materials [10–14].

Furthermore, hydrogen gas sensors were developed using various sensing principles, including optical, electrochemical, and thermal. Optical sensors rely on the interaction of hydrogen molecules with light to produce a measurable signal. Electrochemical sensors use an electrode to detect changes in the concentration of hydrogen gas, while thermal sensors measure temperature changes resulting from the catalytic reaction of hydrogen molecules.

Recently, significant progress was made in developing hydrogen gas sensors that can withstand extreme conditions, including high temperatures, pressure, and humidity. These sensors have the potential to revolutionize the safe storage and transportation of hydrogen fuel.

Therefore, developing a reliable and robust hydrogen gas sensor is essential to ensure the safe storage and transportation of hydrogen fuel. Researchers are actively working on developing novel sensing materials and technologies to overcome the challenges associated with hydrogen gas sensing. With continued research and development, hydrogen fuel may soon become a viable alternative to fossil fuels.

In recent decades, semiconductor hydrogen gas sensors based on AlGaN/GaN] developed rapidly because of their many advantages, such as physical and chemical stability, low cost in mass production, and ability to integrate into the circuit [15–24]. GaN-based gas sensors especially demonstrated excellent capability for extreme environments such as high temperatures and high radiation [25–28]. Compared with the AlGaN/GaN diode type, the HEMT-type sensors exhibited several outstanding advantages, including lower theoretical detection limits, the separation of the current-carrying and the sensing mechanism, and the optimization of the sensor's performance by gate bias modulation [29].

The most crucial component of the sensor is the catalytic structure, which is usually based on metal oxides [30–34] or noble metals [35–39]. Moreover, many studies used the catalyst layer functionalization approach in order to enhance the sensitivity of hydrogen

gas sensors. By pulsed-laser irradiation with an optimizing magnitude of the laser power (75 mJ/cm^2), the NiO thin film exhibited a better response (57.9%) to the hydrogen gas when compared to that of the NiO thin film without irradiation (46.3%) under 3000 ppm of H2 at 175 °C [40]. Other studies developed a p-n metal oxide heterostructure to fabricate high-performance hydrogen gas sensors [41,42]. Additionally, a Pd nanoparticle–decorated SnO_2 nanotubes sensor, which employed the spillover effect of Pd-nanoparticles and porous microstructure of SnO_2, showed a huge improvement in hydrogen gas sensing of 4.3 times higher than that of SnO_2 nanotubes sensor [43]. However, in many cases, the catalyst structure was sensitive to many different gases, leading to the trade-off: the more powerful the catalyst layer, the poorer selectivity, especially for gas sensors using metal oxide catalysts. In order to improve the selectivity of hydrogen gas sensors, the simplest way is to apply a physical filter on the surface of the catalyst material [44,45]. However, to our knowledge, there is no similar study for hydrogen gas sensors based on AlGaN/GaN HEMTs. The reason may lie in the fabrication process, as the AlGaN/GaN HEMTs sensors are fabricated based on photolithography technology. Hence, the application of the thin film on the catalyst layer must be compatible with the fabrication process, which is the major obstacle to the optimization of sensors based on GaN materials.

In this work, we developed a high selectivity hydrogen gas sensor based on AlGaN/GaN HEMTs. A thin layer of WO_3 was deposited on top of the Pd catalyst layer to achieve high selectivity. The sensor worked in a wide range of temperatures and exhibited the highest sensitivity of 658% towards 4% H_2 at 200 °C, while the responses to other gases such as NO_2, CH_4, CO_2, NH_3, and H_2S were comparably low. These results showed that this sensor is promising for H_2 detection in a complex gas environment.

2. Materials and Methods

The gas sensors based on AlGaN/GaN HEMTs were fabricated by the conventional photolithography process at the Inter-University Semiconductor Research Center (ISRC), Seoul, Korea. The AlGaN/GaN-on-Si wafer was purchased as a commercial product, which consisted of a 10 nm in situ SiNx layer, a 22 nm $Al_{0.23}Ga_{0.77}N$ barrier layer, a 0.7 nm AlN nucleation layer, 420 nm i-GaN layer, and buffer layers. First, the source and drain electrodes were patterned by the maskless patterning system, and then, a metal stack of Ti/Al/Ni/Au (20/120/25/50 nm) was deposited by e-beam evaporation. After the lift-off process, the samples were followed by rapid thermal annealing (RTA) at 830 °C for 30 s in N_2 ambient. Next, the mesa isolation at a depth of 300 nm was patterned and applied by inductively coupled plasma (ICP) etching with a BCl_3/Cl_2 mixture to remove the active layers between devices. Then, the gate region was patterned and followed by SiN_x etching by ICP etching with SF_6 plasma. Afterward, a 10 nm Pd layer and a WO_3 layer were formed by e-beam evaporation and a lift-off process on the gate region. In this work, we fabricated 3 samples with different WO_3 thicknesses of 1, 2, and 5 nm (labeled S1, S2, and S3, respectively) to investigate the influence of the WO_3 thickness on hydrogen gas selectivity. Finally, the interconnect bi-layer probing pads of Ti/Au with thicknesses 20/300 nm were formed by e-beam evaporation and lift-off. The dimensions of the gate electrode were 36 μm × 120 μm, the source-gate, and gate-drain spacings were 2 μm. The as-fabricated devices were exposed at 400 °C for 10 min in air for stabilization. The cross-section of the fabrication process is shown in Figure 1.

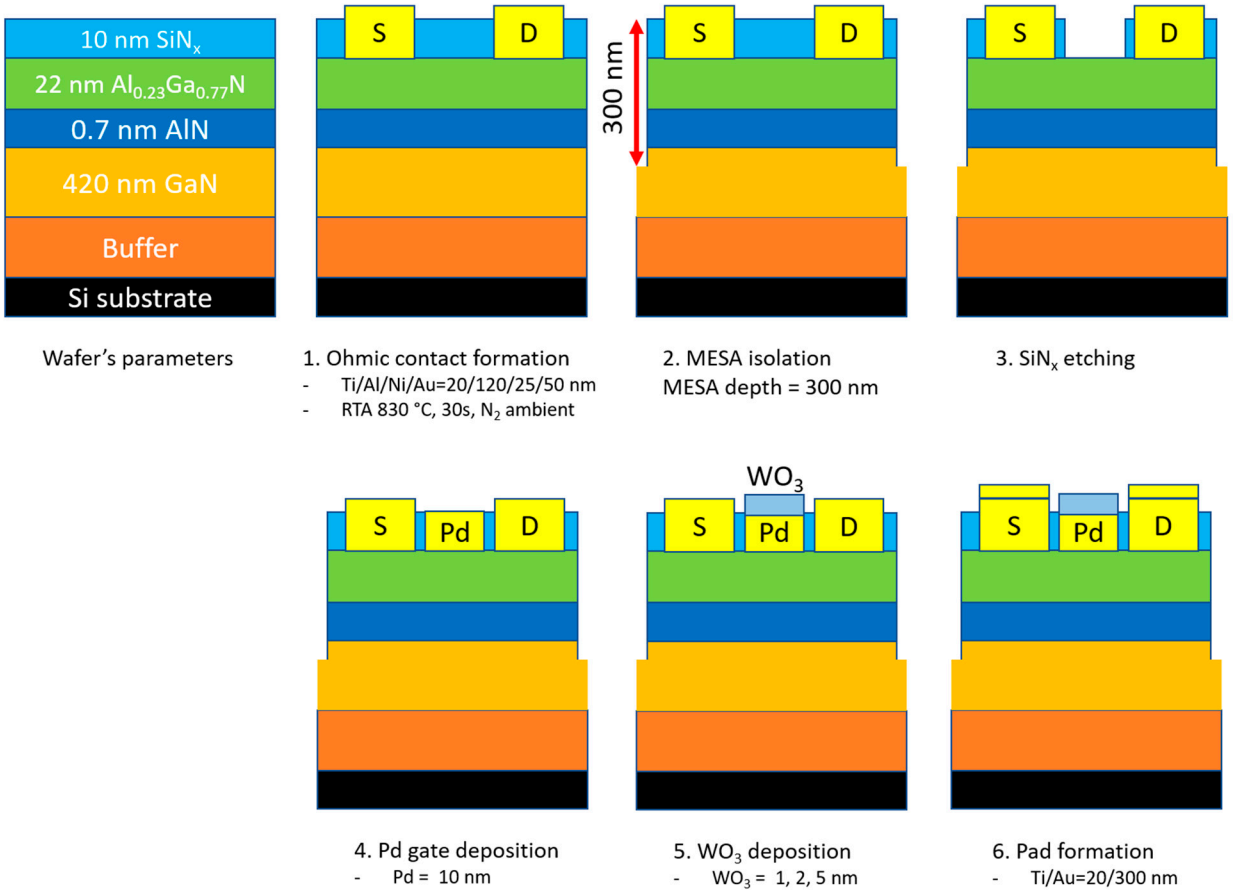

Figure 1. The fabrication process of the Pd-AlGaN/GaN HEMT sensor.

Thin WO_3 film was deposited on a test Si wafer using e-beam evaporator from high purity WO_3 pellets (99.99%) with a Z-ratio of 0.529 [46]. The X-ray photoelectron spectroscopy (XPS) spectra were shown in Figure 2a,b. In Figure 2a, the two main XPS peaks belonged to the typical doublet of W6+ with the binding energy of W ($4f_{7/2}$) centered at 34.9 ± 0.1. On the other hand, the main peak of O (1s) at 530.7 ± 0.1 corresponded to W-O bond (Figure 2b). In addition, the atomic percentage was W:O = 22.24:77.76 (inset of Figure 2b), which is close to the theoretical ratio 25:75, confirming that WO_3 thin film was successfully deposited.

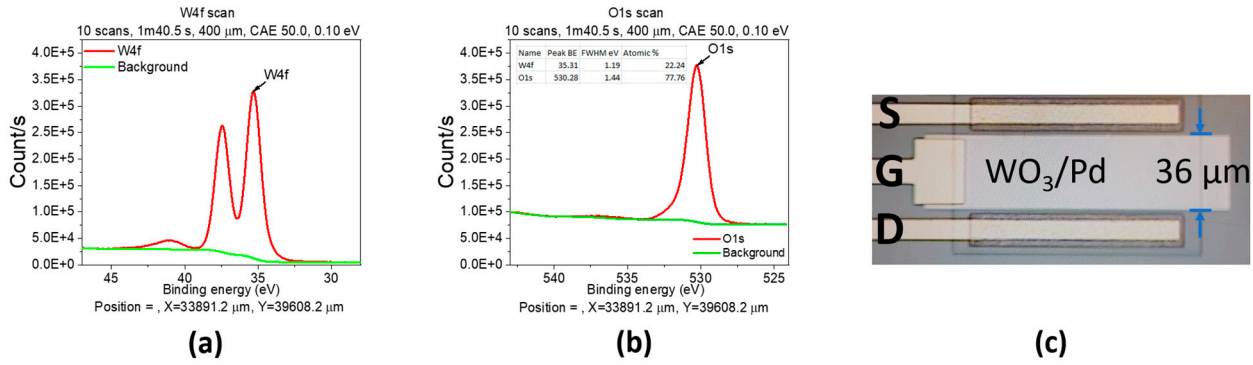

Figure 2. The X-ray photoelectron spectroscopy spectra for W4f and O1s of Si test sample (**a**,**b**) and the microscope image of the fabricated device (**c**).

The microscope image of the fabricated WO_3/Pd-AlGaN/GaN HEMT device was shown in Figure 2c.

The gas sensors based on Pd-AlGaN/GaN were widely investigated and reported [17,18]. When hydrogen molecules came into contact with the Pd catalyst layer, the Pd layer enabled the hydrogen dissociation into hydrogen ions (H+) on the Pd surface. Due to their tiny size, the positively charged hydrogen ions easily diffused through the gate layer via pores and reach the surface of the AlGaN layer. The presence of the positive ions increased the two-dimensional electron gas (2DEG) concentration and lead to an increase in drain current (Figure 3a). The change of conduction band energy with hydrogen exposure was shown in Figure 3b.

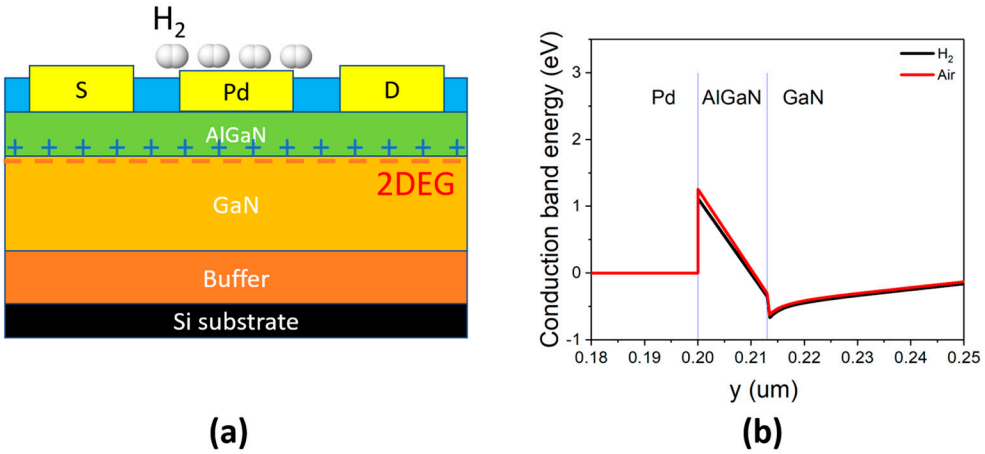

Figure 3. The sensing mechanism of gas sensor based on Pd-AlGaN/GaN HEMT (**a**) and the change of conduction band energy with hydrogen exposure (**b**).

As reported in [47,48], the pure WO_3 thin film exhibited no reduction reaction to H_2 at 50–300 °C. Hence, the thin film of WO_3 acted as a gas filter without compromising Pd's hydrogen sensing and played an essential role in archiving high selectivity for H_2 sensing.

The gas sensor measurement setup was shown in Figure 4. Gas sources consisted of the target gases (H_2, NO_2, CH_4, CO_2, NH_3, and H_2S) and synthesized dry air (O_2/N_2 mixture) as the reference gas. The gas flow was mixed using mass flow controllers (MFCs). The sensors were loaded in a test chamber with a hot chuck to control the operating temperature. Output and gas sensing characteristics were measured by HP 4155A parameter analyzer. The gas flow rate was maintained at 200 sccm in all measurements.

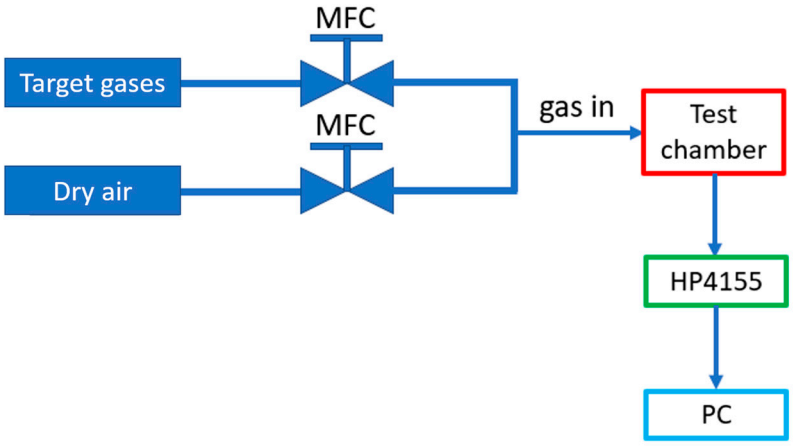

Figure 4. Gas sensor measurement setup.

The relative sensitivity of the sensor was defined by the ratio of the drain current change in the target gas to the base current in dry air:

$$Sensitivity\ (\%) = \frac{|I_0 - I_{gas}|}{I_0} \times 100 = \frac{|\Delta I|}{I_0} \times 100 \quad (1)$$

where I_0 and I_{gas} were the drain current in dry air and target gases, respectively. The response time was defined as the required time for the sensor to reach 90% of the total response from the base current, and the recovery time showed the time required to return to 90% of the base current. The response and recovery times were extracted from the transient characteristics.

3. Results

Figure 5 showed the drain current response to 10 ppm NO_2 at 100, 200, and 300 °C. Our previous work [49] reported that high relative sensitivity towards NO_2 could be achieved in Pd-AlGaN/GaN HEMT sensor by optimizing AlGaN barrier thickness along with gate bias modulation effect. The sensitivity to 10 ppm of NO_2 at 300 °C was 6% at V_G = 0 V and 45.4% at V_G = −1 V, which was much improved in the sensor device with 13 nm AlGaN barrier. However, a thin layer of WO_3 deposited on top of the Pd layer made the sensors remarkably less sensitive to NO_2 as shown in Figure 5. When Pd gate was covered with 1 nm of WO_3, the S1 sensor still demonstrated the sensitivity of 8.9%, 18.4%, and 17.2% at 100, 200, and 300 °C, respectively. However, NO_2 response was diminished significantly in the S2 sensor with 2 nm- WO_3 layer (Figure 5b), and the S3 sensor with 5 nm WO_3 lost the NO_2 sensitivity completely (Figure 5c). The NO_2 insensitivity indicated that the WO_3 layer can be utilized as a gas filter against NO_2. When this filter layer was thick enough beyond 5 nm thickness, the sensor was no longer sensitive to NO_2. In this work, we found that 5 nm of WO_3 was enough for NO_2 insensitivity, while maintaining working stability. Although the WO_3 thin film was reported to be sensitive to NO_2 [50,51], our data showed that the WO_3/Pd dual layer did not have any enhancement for the NO_2 sensing.

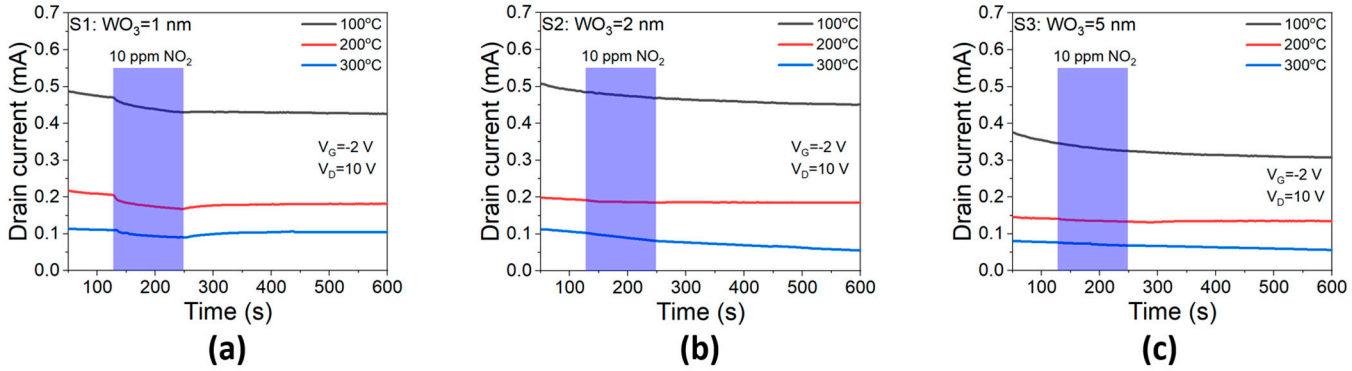

Figure 5. Response to 10 ppm NO_2 of the sensors at different temperatures. (**a**) 1 nm (**b**) 2 nm (**c**) 5 nm of WO_3 layer.

The WO_3/Pd-AlGaN/GaN hydrogen gas sensor operated normally in a wide range of temperatures from 25 °C to 250 °C, as shown in Figure 6. At 200 °C, the S3 sensor exhibited the highest relative sensitivity (Figure 6f). These results were similar to other works using Pd-AlGaN/GaN HEMTs sensor. This result indicated that the WO_3 layer on Pd catalyst did not affect the hydrogen gas sensing mechanism.

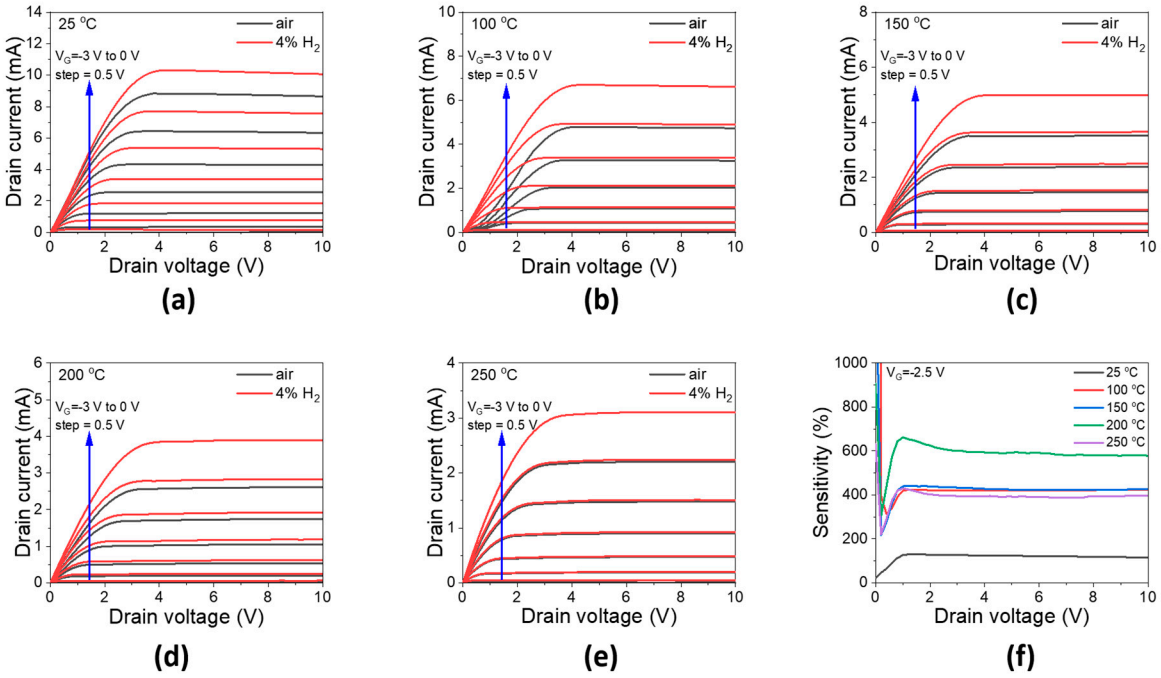

Figure 6. Output characteristics of the S3 sensor in air and 4% H_2 gas from (**a**) 25, (**b**) 100, (**c**) 150, (**d**) 200, and (**e**) 250 °C at different gate voltages from −3 V to 0 V. (**f**) the sensitivity extracted from output characteristics at gate voltage of −2.5 V.

The thin WO_3 layer, which acted as a filter or a blocking layer, might degrade the sensor's performance. However, the WO_3/Pd-AlGaN/GaN HEMT sensor maintained a high performance for hydrogen sensing, as shown in Figure 7. At 200 °C, the transient characteristics of the sensor showed a fast response (12 s) and recovery times (4 s) while maintaining the high sensitivity of 658% under hydrogen gas of 4% concentration.

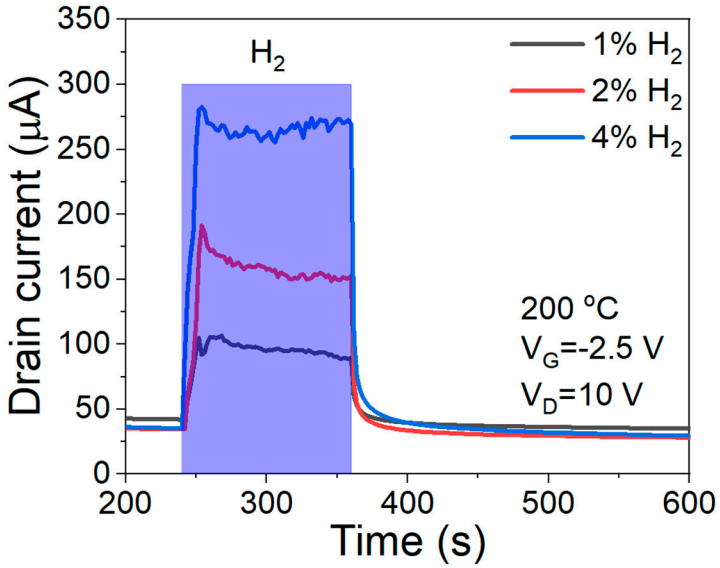

Figure 7. Response to H_2 gas of S3 sensor at 200 °C.

The sensitivity of the sensors was measured with the same bias point and temperature under exposure to various gases, including NO_2, CH_4, CO_2, NH_3, and H_2S, in order to evaluate the hydrogen selectivity. Unfortunately, the measurement was not conducted in the gas combining condition, due to the limitation of the measurement facility. The

sensitivity of our sensors to many different gases was shown in Figure 8. To our knowledge, the hydrogen gas sensor based on AlGaN/GaN with such a high selectivity was rarely reported. The high selectivity of the sensor can be explained by the combination of a high hydrogen-sensitive catalyst and the filter effect of the WO_3 layer. First, being the smallest gas molecule with a bond length of 0.74 Å [52], hydrogen gas molecules can easily diffuse and penetrate the filter. A similar filter approach was investigated to achieve high hydrogen selectivity. For example, a low porosity of SiO_2 layer, as a molecular sieve, enhanced the hydrogen selectivity of SnO_2 thick film [53]. Similarly, SnO_2 gas sensors with SiO_2 deposited on the surface showed significant improvement in hydrogen selectivity, whereas no noticeable response toward ethanol, acetone, and benzene were detected [54]. Second, palladium itself is a powerful catalyst with a high affinity toward hydrogen, which allows the effective dissociation of hydrogen molecules into hydrogen atoms and forms the palladium hydrides PdH_x [55,56].

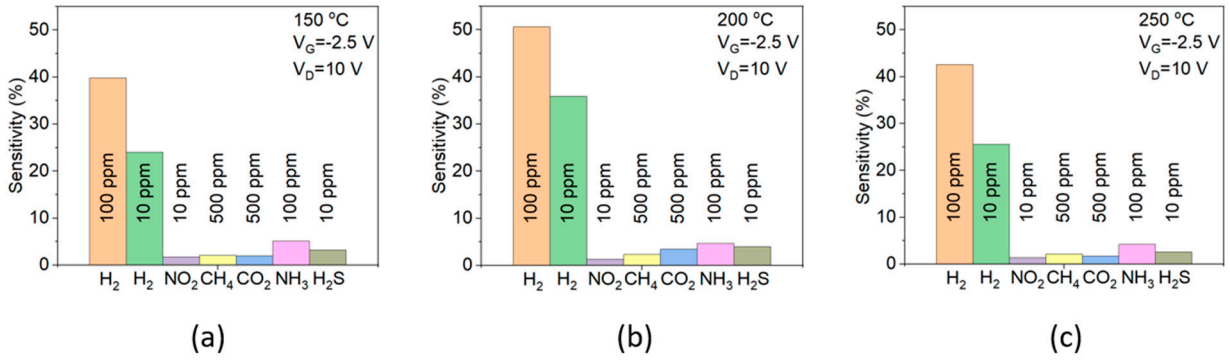

Figure 8. Hydrogen selectivity of S3 sensor at 150 °C (**a**), 200 °C (**b**), and 250 °C (**c**).

The stability of S3 sensor was exhibited by the transfer characteristics at 200 °C, as shown in Figure 9. After 4 months with various measurements, we observed roughly 7% of the current collapse.

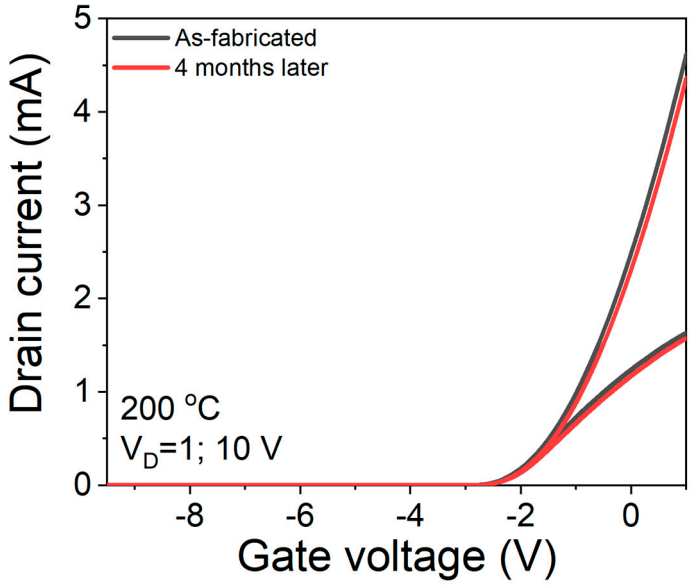

Figure 9. Stability of S3 sensor.

4. Conclusions

We reported a high selectivity hydrogen gas sensor based on AlGaN/GaN HEMTs. A thin layer of WO_3 on top of the Pd layer worked as a gas filter to enhance the sensor selectivity towards hydrogen gas. High selectivity and sensitivity, fast response, and quick

recovery times made the sensor ideal for hydrogen gas sensing at a high temperature in a complex gas environment.

Author Contributions: Experiment, analysis, measurement, and writing, V.C.N.; project administration, H.-Y.C.; methodology, validation, review, funding acquisition, and supervision, H.K. All authors have read and agreed to the published version of the manuscript.

Funding: This work was supported by Basic Science Research Programs (2015R1A6A1A03031833, 2021R1F1A1051094) through the National Research Foundation of Korea (NRF). This research was also supported by the National R&D Program through the NRF funded by the Ministry of Science and ICT (2022M3I8A1077243).

Institutional Review Board Statement: This study did not require ethical approval.

Informed Consent Statement: Not applicable.

Data Availability Statement: Not applicable.

Acknowledgments: The sensor measurements with gases other than H_2 and NO_2 were carried out in Electronics Materials and Devices Lab of Kyungpook National University.

Conflicts of Interest: The authors declare no conflict of interest.

References

1. Archer, D.; Brovkin, V. The millennial atmospheric lifetime of anthropogenic CO_2. *Clim. Chang.* **2008**, *90*, 283–297. [CrossRef]
2. Ebi, K.L.; Hallegatte, S.; Kram, T.; Arnell, N.W.; Carter, T.R.; Edmonds, J.; Kriegler, E.; Mathur, R.; O'Neill, B.C.; Riahi, K.; et al. A new scenario framework for climate change research: Background, process, and future directions. *Clim. Chang.* **2014**, *122*, 363–372. [CrossRef]
3. Hawkins, E.; Ortega, P.; Suckling, E.; Schurer, A.; Hegerl, G.; Jones, P.; Joshi, M.; Osborn, T.J.; Masson-Delmotte, V.; Mignot, J.; et al. Estimating Changes in Global Temperature since the Preindustrial Period. *Bull. Am. Meteorol. Soc.* **2017**, *98*, 1841–1856. [CrossRef]
4. Ehlert, D.; Zickfeld, K. What determines the warming commitment after cessation of CO_2 emissions? *Environ. Res. Lett.* **2017**, *12*, 015002. [CrossRef]
5. King, A.D.; Donat, M.G.; Lewis, S.C.; Henley, B.J.; Mitchell, D.M.; Stott, P.A.; Fischer, E.M.; Karoly, D.J. Reduced heat exposure by limiting global warming to 1.5 °C. *Nat. Clim. Chang.* **2018**, *8*, 549–551. [CrossRef]
6. Döll, P.; Trautmann, T.; Gerten, D.; Schmied, H.M.; Ostberg, S.; Saaed, F.; Schleussner, C.-F. Risks for the global freshwater system at 1.5 °C and 2 °C global warming. *Environ. Res. Lett.* **2018**, *13*, 044038. [CrossRef]
7. Available online: https://www.esrl.noaa.gov/gmd/ccgg/trends/ (accessed on 8 March 2022).
8. Cane, M.A.; Clement, A.C.; Kaplan, A.; Kushnir, Y.; Pozdnyakov, D.; Seager, R.; Zebiak, S.E.; Murtugudde, R. Twentieth-Century Sea Surface Temperature Trends. *Science* **1997**, *275*, 957–960. [CrossRef]
9. Pollack, H.N.; Huang, S.; Shen, P.-Y. Climate Change Record in Subsurface Temperatures: A Global Perspective. *Science* **1998**, *282*, 279–281. [CrossRef]
10. DiMeo, F.; Chen, I.; Chen, P.; Neuner, J.; Roerhl, A.; Welch, J. MEMS-based hydrogen gas sensors. *Sens. Actuators B Chem.* **2006**, *117*, 10–16. [CrossRef]
11. Wong, Y.M.; Kang, W.P.; Davidson, J.L.; Wisitsora-at, A.; Soh, K.L. A novel microelectronic gas sensor utilizing carbon nanotubes for hydrogen gas detection. *Sens. Actuators B Chem.* **2003**, *93*, 327–332. [CrossRef]
12. Lupan, O.; Chai, G.; Chow, L. Novel hydrogen gas sensor based on single ZnO nanorod. *Microelectron. Eng.* **2008**, *85*, 2220–2225. [CrossRef]
13. Kaniyoor, A.; Imran Jafri, R.; Arockiadoss, T.; Ramaprabhu, S. Nanostructured Pt decorated graphene and multi walled carbon nanotube based room temperature hydrogen gas sensor. *Nanoscale* **2009**, *1*, 382–386. [CrossRef]
14. Nakagomi, S.; Sai, T.; Kokubun, Y. Hydrogen gas sensor with self temperature compensation based on β-Ga_2O_3 thin film. *Sens. Actuators B Chem.* **2013**, *187*, 413–419. [CrossRef]
15. Kang, B.S.; Ren, F.; Gila, B.P.; Abernathy, C.R.; Pearton, S.J. AlGaN/GaN-based metal–oxide–semiconductor diode-based hydrogen gas sensor. *Appl. Phys. Lett.* **2004**, *84*, 1123–1125. [CrossRef]
16. Song, J.; Lu, W.; Flynn, J.S.; Brandes, G.R. AlGaN/GaN Schottky diode hydrogen sensor performance at high temperatures with different catalytic metals. *Solid State Electron.* **2005**, *49*, 1330–1334. [CrossRef]
17. Hung, S.-T.; Chang, C.-J.; Hsu, C.-H.; Chu, B.H.; Lo, C.F.; Hsu, C.-C.; Pearton, S.J.; Holzworth, M.R.; Whiting, P.G.; Rudawski, N.G.; et al. SnO_2 functionalized AlGaN/GaN high electron mobility transistor for hydrogen sensing applications. *Int. J. Hydrog. Energy* **2012**, *37*, 13783–13788. [CrossRef]
18. Zhong, A.; Sun, A.; Shen, B.; Yu, H.; Zhou, Y.; Liu, Y.; Xie, Y.; Luo, J.; Zhang, D.; Fan, P. Tailoring the H_2 gas detection range of the AlGaN/GaN high electron mobility transistor by tuning the Pt gate thickness. *Int. J. Hydrog. Energy* **2022**, *47*, 2050–2058. [CrossRef]

19. Ahn, J.; Kim, D.; Park, K.-H.; Yoo, G.; Heo, J. Pt-Decorated Graphene Gate AlGaN/GaN MIS-HEMT for Ultrahigh Sensitive Hydrogen Gas Detection. *IEEE Trans. Electron. Devices* **2021**, *68*, 1255–1261. [CrossRef]
20. Chung, G.H.; Vuong, T.A.; Kim, H. Demonstration of hydrogen sensing operation of AlGaN/GaN HEMT gas sensors in extreme environment. *Results Phys.* **2019**, *12*, 83–84. [CrossRef]
21. Sun, A.; Yu, H.; Zhou, Y.; Liu, Y.; Luo, J.; Fan, P.; Zhong, A. Pd gated AlGaN/GaN high electron mobility transistor for ppb level hydrogen gas detection. *Int. J. Hydrog. Energy* **2022**, *47*, 17494–17503. [CrossRef]
22. Choi, J.-H.; Jo, M.-G.; Han, S.-W.; Kim, H.; Kim, S.-H.; Jang, S.; Kim, J.-S.; Cha, H.-Y. Hydrogen gas sensor of Pd-functionalised AlGaN/GaN heterostructure with high sensitivity and low-power consumption. *Electron. Lett.* **2017**, *53*, 1200–1202. [CrossRef]
23. Shen, B.; Luo, J.; Xie, Y.; Zhang, D.; Fan, P.; Zhong, A. Hydrogen gas ppb-level detection based on AlGaN/GaN high electron mobility transistor with 2.0 nm thick Pt gate layer. *Appl. Phys. Lett.* **2019**, *115*, 254104. [CrossRef]
24. Tsai, T.-H.; Chen, H.-I.; Liu, I.-P.; Hung, C.-W.; Chen, T.-P.; Chen, L.-Y.; Liu, Y.-J.; Liu, W.-C. Investigation on a Pd–AlGaN/GaN Schottky Diode-Type Hydrogen Sensor with Ultrahigh Sensing Responses. *IEEE Trans. Electron. Devices* **2008**, *55*, 3575–3581. [CrossRef]
25. Kang, B.; Wang, H.-T.; Tien, L.-C.; Ren, F.; Gila, B.; Norton, D.; Abernathy, C.; Lin, J.; Pearton, S. Wide Bandgap Semiconductor Nanorod and Thin Film Gas Sensors. *Sensors* **2006**, *6*, 643–666. [CrossRef]
26. Halfaya, Y.; Bishop, C.; Soltani, A.; Sundaram, S.; Aubry, V.; Voss, P.; Salvestrini, J.-P.; Ougazzaden, A. Investigation of the Performance of HEMT-Based NO, NO_2 and NH_3 Exhaust Gas Sensors for Automotive Antipollution Systems. *Sensors* **2016**, *16*, 273. [CrossRef]
27. Vuong, T.-A.; Cha, H.-Y.; Kim, H. Response Enhancement of Pt–AlGaN/GaN HEMT Gas Sensors by Thin AlGaN Barrier with the Source-Connected Gate Configuration at High Temperature. *Micromachines* **2021**, *12*, 537. [CrossRef]
28. Ranjan, A.; Agrawal, M.; Radhakrishnan, K.; Dharmarasu, N. AlGaN/GaN HEMT-based high-sensitive NO_2 gas sensors. *Jpn. J. Appl. Phys.* **2019**, *58*, SCCD23. [CrossRef]
29. Bishop, C.; Halfaya, Y.; Soltani, A.; Sundaram, S.; Li, X.; Streque, J.; el Gmili, Y.; Voss, P.L.; Salvestrini, J.P.; Ougazzaden, A. Experimental Study and Device Design of NO, NO_2, and NH_3 Gas Detection for a Wide Dynamic and Large Temperature Range Using Pt/AlGaN/GaN HEMT. *IEEE Sens. J.* **2016**, *16*, 6828–6838. [CrossRef]
30. Rýger, I.; Vanko, G.; Kunzo, P.; Lalinský, T.; Vallo, M.; Plecenik, A.; Satrapinský, L.; Plecenik, T. AlGaN/GaN HEMT Based Hydrogen Sensors with Gate Absorption Layers Formed by High Temperature Oxidation. *Procedia Eng.* **2012**, *47*, 518–521. [CrossRef]
31. Lee, J.; Kim, D.H.; Hong, S.; Jho, J.Y. A hydrogen gas sensor employing vertically aligned TiO_2 nanotube arrays prepared by template-assisted method. *Sens. Actuators B Chem.* **2011**, *160*, 1494–1498. [CrossRef]
32. Matsumiya, M.; Qiu, F.; Shin, W.; Izu, N.; Murayama, N.; Kanzaki, S. Thin-film Li-doped NiO for thermoelectric hydrogen gas sensor. *Thin Solid Films* **2002**, *419*, 213–217. [CrossRef]
33. Li, H.; Wu, C.; Liu, Y.; Yuan, S.; Chiang, Z.; Zhang, S.; Wu, R. Mesoporous WO_3-TiO_2 heterojunction for a hydrogen gas sensor. *Sens. Actuators B Chem.* **2021**, *341*, 130035. [CrossRef]
34. Mondal, B.; Basumatari, B.; Das, J.; Roychaudhury, C.; Saha, H.; Mukherjee, N. ZnO–SnO_2 based composite type gas sensor for selective hydrogen sensing. *Sens. Actuators B Chem.* **2014**, *194*, 389–396. [CrossRef]
35. Lee, E.; Hwang, I.; Cha, J.; Lee, H.; Lee, W.; Pak, J.J.; Lee, J.; Ju, B. Micromachined catalytic combustible hydrogen gas sensor. *Sens. Actuators B Chem.* **2011**, *153*, 392–397. [CrossRef]
36. Matsumiya, M.; Shin, W.; Izu, N.; Murayama, N. Nano-structured thin-film Pt catalyst for thermoelectric hydrogen gas sensor. *Sens. Actuators B Chem.* **2003**, *93*, 309–315. [CrossRef]
37. Kim, K.T.; Sim, J.; Cho, S.M. Hydrogen gas sensor using Pd nanowires electro-deposited into anodized alumina template. *IEEE Sens. J.* **2006**, *6*, 509–513.
38. Yoon, J.; Kim, B.; Kim, J. Design and fabrication of micro hydrogen gas sensors using palladium thin film. *Mater. Chem. Phys.* **2012**, *133*, 987–991. [CrossRef]
39. Im, Y.; Lee, C.; Vasquez, R.; Bangar, M.; Myung, N.; Menke, E.; Penner, R.; Yun, M. Investigation of a Single Pd Nanowire for Use as a Hydrogen Sensor. *Small* **2006**, *2*, 356–358. [CrossRef]
40. Soleimanpour, A.M.; Khare, S.V.; Jayatissa, A.H. Enhancement of Hydrogen Gas Sensing of Nanocrystalline Nickel Oxide by Pulsed-Laser Irradiation. *ACS Appl. Mater. Interfaces* **2012**, *4*, 4651–4657. [CrossRef]
41. Lee, J.-H.; Kim, J.-Y.; Mirzaei, A.; Kim, H.; Kim, S. Significant Enhancement of Hydrogen-Sensing Properties of ZnO Nanofibers through NiO Loading. *Nanomaterials* **2018**, *8*, 902. [CrossRef]
42. Hazra, S.K.; Basu, S. Hydrogen sensitivity of ZnO p–n homojunctions. *Sens. Actuators B Chem.* **2006**, *117*, 177–182. [CrossRef]
43. Cai, Z.; Park, S. A superior sensor consisting of porous, Pd nanoparticle–decorated SnO_2 nanotubes for the detection of ppb-level hydrogen gas. *J. Alloys Compd.* **2022**, *907*, 164459. [CrossRef]
44. Weh, T.; Fleischer, M.; Meixner, H. Optimization of physical filtering for selective high temperature H_2 sensors. *Sens. Actuators B Chem.* **2000**, *68*, 146–150. [CrossRef]
45. Nguyen, V.T.; Chu, M.H.; Nguyen, D.H.; Nguyen, V.D.; Dang, T.T.L.; Nguyen, T.T.H.; Nguyen, N.V.; Phan, H.P.; Nguyen, V.H. Enhanced NH_3 and H_2 gas sensing with H_2S gas interference using multilayer SnO_2/Pt/WO_3 nanofilms. *J. Hazard. Mater.* **2021**, *412*, 125181.

46. Lim, S.H.; Kim, H.K. Deposition Rate Effect on Optical and Electrical Properties of Thermally Evaporated WO_{3-x}/Ag/WO_{3-x} Multilayer Electrode for Transparent and Flexible Thin Film Heaters. *Sci. Rep.* **2020**, *10*, 8357. [CrossRef] [PubMed]
47. Zhang, C.; Boudiba, A.; Olivier, M.; Snyders, R.; Debliquy, M. Magnetron sputtered tungsten oxide films activated by dip-coated platinum for ppm-level hydrogen detection. *Thin Solid Films* **2012**, *520*, 3679–3683. [CrossRef]
48. Zhang, C.; Boudiba, A.; Olivier, M.; Snyders, R.; Debliquy, M. Sensing properties of Pt/Pd activated tungsten oxide films grown by simultaneous radio-frequency sputtering to reducing gases. *Sens. Actuators B Chem.* **2012**, *175*, 53–59. [CrossRef]
49. Nguyen, V.C.; Kim, K.; Kim, H. Performance Optimization of Nitrogen Dioxide Gas Sensor Based on Pd-AlGaN/GaN HEMTs by Gate Bias Modulation. *Micromachines* **2021**, *12*, 400. [CrossRef]
50. Cantalini, C.; Sun, H.; Faccio, M.; Pelino, M.; Santucci, S.; Lozzi, L.; Passacantando, M. NO_2 sensitivity of WO_3 thin film obtained by high vacuum thermal evaporation. *Sens. Actuators B Chem.* **1996**, *31*, 81–87. [CrossRef]
51. Prajapati, C.S.; Bhat, N. ppb level detection of NO_2 using a WO_3 thin film-based sensor: Material optimization, device fabrication and packaging. *RSC Adv.* **2018**, *8*, 6590–6599. [CrossRef]
52. DeKock, R.L.; Gray, H.B. *Chemical Structure and Bonding*; University Science Books: New York, NY, USA, 1989; p. 85.
53. Tournier, G.; Pijolat, C. Selective filter for SnO-based gas sensor: Application to hydrogen trace detection. *Sens. Actuators B Chem.* **2005**, *106*, 553–562. [CrossRef]
54. Meng, X.; Zhang, Q.; Zhang, S.; He, Z. The Enhanced H_2 Selectivity of SnO_2 Gas Sensors with the Deposited SiO_2 Filters on Surface of the Sensors. *Sensors* **2019**, *19*, 2478. [CrossRef] [PubMed]
55. Patton, J.F.; Hunter, S.R.; Sepaniak, M.J.; Daskos, P.G.; Smith, D.B. Rapid response microsensor for hydrogen detection using nanostructured palladium films. *Sens. Actuator A Phys.* **2010**, *163*, 464–470. [CrossRef]
56. Korotcenkov, G. *Handbook of Gas Sensor Materials*; Springer: New York, NY, USA, 2013; pp. 153–163.